JOURNAL OF MATERIALS SCIENCE 17 (1982) 3211–3220

Stiffness and strength behaviour of woven fabric composites

T. ISHIKAWA*, T.-W. CHOU
Mechanical and Aerospace Engineering Department, University of Delaware, Newark, Delaware 19711, USA

This paper presents three analytical models for the investigation of the stiffness and strength of woven fabric composites. The "mosaic model" is effective in predicting the elastic properties of fabric composites. The "fibre undulation model" takes into account fibre continuity and undulation and has been adopted for modelling the "knee behaviour" of plain weave fabric composites. The "bridging model" is developed to simulate the load transfer among the interlaced regions in satin composites. The theoretical predictions coincide extremely well with experimental measurements. The elastic stiffness and knee stress in satin composites are higher than those in plain weave composites due to the presence of the bridging regions in the weaving pattern.

1. Introduction

Woven fabric composites have gained increasing technological importance. They provide more balanced properties in the fabric plane than unidirectional laminae; the bidirectional reinforcement in a single layer of fabric gives rise to excellent impact resistance. The ease of handling and low fabrication cost have made fabrics attractive for structural applications [1–3].

In spite of their popularity, the mechanical behaviour of fabric composites is not well understood. The purposes of this paper are two-fold. First, the linear elastic properties of woven fabric composites are predicted. Second, the non-linear behaviour due to the initial failure of the fabric, which is known as the "knee phenomenon" [4], is modelled and analysed.

All woven fabrics consist of two sets of interlaced threads, known as the warp and fill threads [5]. The types of fabrics can be identified by the pattern of repeat of the interlaced regions as shown in Fig. 1. Two basic geometrical parameters can be defined to characterize a fabric; n_{fg} denotes that a warp thread is interlaced with every n_{fg}-th fill thread and n_{wg} denotes that a fill thread is interlaced with every n_{wg}-th warp thread. Here, we confine ourselves to non-hybrid fabrics and the case of $n_{wg} = n_{fg} = n_g$. Fabrics with $n_g \geqslant 4$ and where the interlaced regions are not connected are known as satin weaves. As defined by their n_g values, the fabrics in Fig. 1 are termed plain weave ($n_g = 2$), twill weave ($n_g = 3$), 4 harness satin ($n_g = 4$), and 8 harness satin ($n_g = 8$).

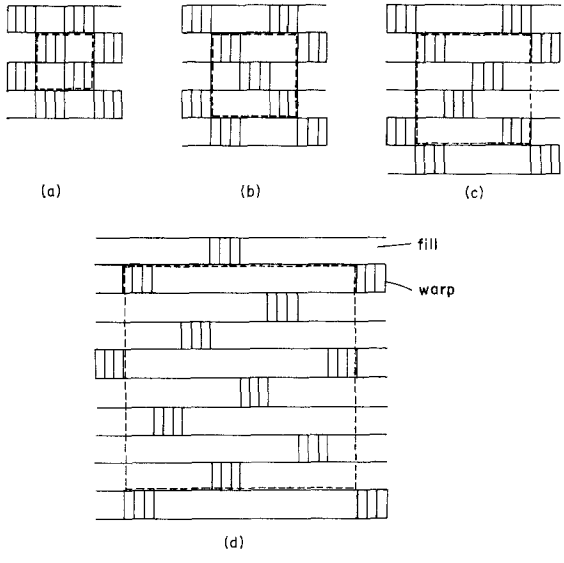

Figure 1 Examples of woven fabric patterns: (a) plain weave ($n_g = 2$); (b) twill weave ($n_g = 3$); (c) 4 harness satin ($n_g = 4$); and (d) 8 harness satin ($n_g = 8$).

*On leave from National Aerospace Laboratory 1880 Jindaiji, Chofu, Tokyo, 182, Japan.

0022–2461/82/113211–10$03.70/0

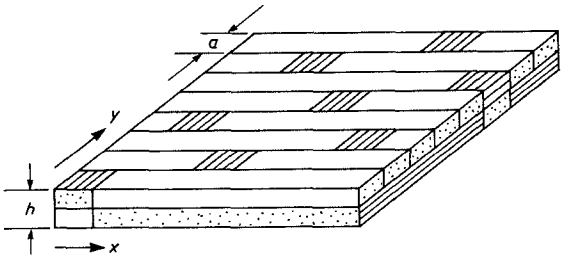

Figure 2 Idealization for the mosaic model. (a) cross-sectional view of a woven fabric, (b) woven fabric impregnated with resin, (b) idealization of the fabric composite.

The authors have proposed and developed three models for approximating the elastic and knee behaviour of woven fabric composites. In the first model, also referred to as the "mosaic model", a woven fabric (Fig. 2a) after impregnation with resin (Fig. 2b) is idealized as an assemblage of asymmetrical cross-ply laminates. Fig. 3 depicts the two-dimensional view of the mosaic model for a woven fabric composite. By combining this model and the iso-stress and iso-strain assumptions, the upper and lower bounds of elastic moduli have been derived by Ishikawa [6], and Ishikawa and Chou [7] for non-hybrid and hybrid fabric composites, respectively. The scheme based upon the mosaic model is different from that of some existing theories [8–10] in that we have adopted the classical laminated plate theory as the basis of the analysis and have provided simple closed form expressions of the bounds. The predictions for hybrid fabric composites in [7] compare very favourably with experimental results of [2].

The objective of the second model is to assess the validity and applicability of the mosaic model, where the fibre undulation and continuity have been omitted. The fibre "undulation model" shown in Fig. 4, therefore, has been introduced by Ishikawa and Chou [11], for analysing the

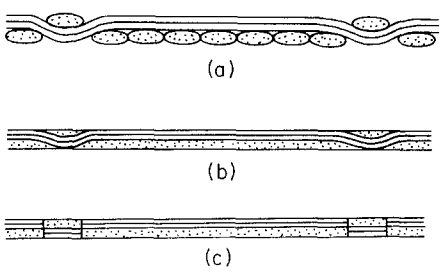

Figure 3 Mosaic model of a repeating unit for an 8 harness satin.

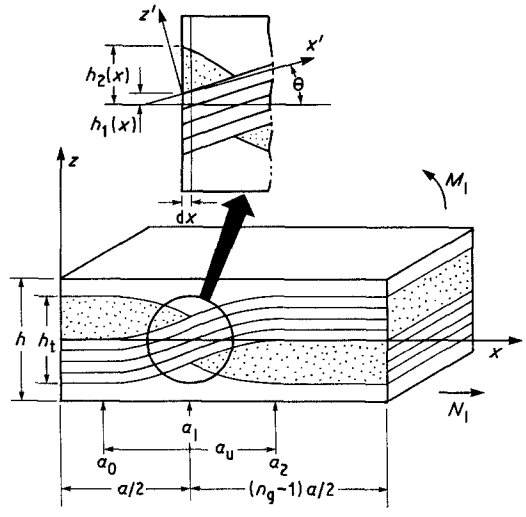

Figure 4 Fibre undulation model.

elastic and knee behaviour of a threadwise strip of a fabric composite. A brief description of the model of [11] and its refinement is given in Section 2. The essential assumption in this approach is that the classical laminated plate theory is applicable to each infinitesimal piece of the threadwise strip. The knee behaviour is then investigated based upon the undulation model with the further assumption of the successive failure of threads transverse to the applied load.

The success of the threadwise idealization has led to the idea of the third model, known as a "bridging model", for the analysis of mechanical properties of satin composites. A schematic view of the bridging model is depicted in Fig. 8c for a repeating unit of the satin fabric composite. The regions with straight threads (denoted by A, B, D and E) have higher local in-plane stiffness than that of an interlaced region (denoted by C) surrounded by them and hence act as load-carrying bridges between adjacent interlaced regions. Finally, the knee behaviour in general satin composites is analysed by combining this model with the approach of successive thread failure.

2. Fibre undulation model for threadwise analysis

The fibre undulation model is developed in order to consider the continuity and undulation of fibres in a fabric composite. Although the formulation of the problem developed in the following is applicable to n_g values in general, the purpose of this model here is to explain the behaviour of

plain weave composites where $n_g = 2$, and to provide the basis of the bridging model to be developed later. For predicting the behaviour of satin composites where $n_g \geqq 4$, we shall employ the bridging model, and the reason will be given in Section 4. Fig. 4 depicts the geometry of the model where the undulation shape is defined by the parameters $h_1(x)$, $h_2(x)$ and a_u. The parameters $a_0 = (a - a_u)/2$ and $a_2 = (a + a_u)/2$ are automatically determined by specifying a_u, which is geometrically arbitrary in the range from 0 to a. Because a pure matrix region appears in the model, an "overall" fibre volume fraction, V_f can be different from V_f in the thread region.

To simulate the actual configuration, the following form of undulation is assumed for the fill thread

$$h_1(x) = \begin{cases} 0 & (0 \leqq x \leqq a_0) \\ \left[1 + \sin\left\{\left(x - \frac{a}{2}\right)\frac{\pi}{a_u}\right\}\right] h_t/4 & (a_0 \leqq x \leqq a_2) \\ h_t/2 & (a_2 \leqq x \leqq n_g a/2) \end{cases} \quad (1)$$

The sectional shape of the warp thread is expressed by

$$h_2(x) = \begin{cases} h_t/2 & (0 \leqq x \leqq a_0) \\ \left[1 - \sin\left\{\left(x - \frac{a}{2}\right)\frac{\pi}{a_u}\right\}\right] h_t/4 & (a_0 \leqq x \leqq a/2) \\ -\left[1 + \sin\left\{\left(x - \frac{a}{2}\right)\frac{\pi}{a_u}\right\}\right] h_t/4 & (a/2 \leqq x \leqq a_2) \\ -h_t/2 & (a_2 \leqq x \leqq n_g a/2). \end{cases} \quad (2)$$

Equation 2 represents an improvement of the form of $h_2(x)$ originally proposed in [11]. The refinement is made based upon the observation of an actual section as depicted in [8].

The theoretical basis of the present investigation is the classical laminated plate theory [12, 13]. The constitutive equations are given by

$$\begin{pmatrix} N_i \\ M_i \end{pmatrix} = \begin{bmatrix} A_{ij} & B_{ij} \\ B_{ij} & D_{ij} \end{bmatrix} \begin{pmatrix} \epsilon_j^0 \\ \kappa_j \end{pmatrix}, \quad (3a)$$

where

$$(A_{ij}, B_{ij}, D_{ij}) = \sum_{m-1}^{4} \int_{h_{m-1}}^{h_m} (1, z, z^2) Q_{ij} \, dZ \quad (3b)$$

and

$$Q_{ij} = \begin{bmatrix} E_x/D_\nu & \nu_{xy}E_x/D_\nu & 0 \\ \nu_{yx}E_y/D_\nu & E_y/D_\nu & 0 \\ 0 & 0 & G_{xy} \end{bmatrix} \quad (3c)$$

$$D_\nu = 1 - \nu_{yx}\nu_{xy}. \quad (3d)$$

In Equation 3b the Q_{ij} is evaluated based upon the corresponding stiffness properties within the layer defined by h_m and h_{m-1}. This is shown in Equation 5. As the inverted form of Equation 3a, we have

$$\begin{pmatrix} \epsilon_i^0 \\ \kappa_i \end{pmatrix} = \begin{bmatrix} a_{ij}^* & b_{ij}^* \\ b_{ij}^* & d_{ij}^* \end{bmatrix} \begin{pmatrix} N_j \\ M_j \end{pmatrix}, \quad (4)$$

where N_i, M_i, ϵ_i^0 and κ_i indicate membrane stress resultants, moment resultants, strain, and curvature of the laminate geometrical midplane, respectively. It is assumed that this theory is applicable to each infinitesimal piece of the model along the x-axis. Thus, A_{ij}, B_{ij} and D_{ij} are expressed as functions of x $(0 \leqq x \leqq a/2)$ by

$$\begin{aligned} A_{ij}(x) &= \int_{-h/2}^{h_1(x)-h_t/2} Q_{ij}^{M} \, dz + \int_{h_1(x)-h_t/2}^{h_1(x)} Q_{ij}^{F}(\theta) \, dz \\ &\quad + \int_{h_1(x)}^{h_2(x)} Q_{ij}^{W} \, dz + \int_{h_2(x)}^{h/2} Q_{ij}^{M} \, dz \\ &= Q_{ij}^{M}(h_1(x) - h_2(x) + h - h_t/2) \\ &\quad + Q_{ij}^{F}(\theta) h_t/2 + Q_{ij}^{W}(h_2(x) - h_1(x)) \end{aligned} \quad (5)$$

$$B_{ij}(x) = \tfrac{1}{2} Q_{ij}^{F}(\theta)\,[h_1(x) - h_t/4]\,h_t + \tfrac{1}{4} Q_{ij}^{W}\,[h_2(x) - h_1(x)]\,h_t \quad (6)$$

$$D_{ij}(x) = \tfrac{1}{3} Q_{ij}^{M}\,\{[h_1(x) - h_t/2]^3 - h_2(x)^3 + h^3/4\} + \tfrac{1}{3} Q_{ij}^{F}(\theta)\,[h_t^3/8 - 3h_t^2 h_1(x)/4 + 3h_t h_1^2(x)/2] + \tfrac{1}{3} Q_{ij}^{W}\,[h_2(x)^3 - h_1(x)^3], \quad (7)$$

where superscripts F, W and M signify the fill and warp threads and matrix, respectively. Similar expressions can be written for $a/2 \leqq x \leqslant n_g a/2$. The local stiffness of the fill, $Q_{ij}^{F}(\theta)$, appearing in Equations 5 to 7 is calculated as a function of the local off-axis angle, $\theta(x)$, which is defined as

$$\theta(x) = \arctan\left(\frac{\mathrm{d}h_1(x)}{\mathrm{d}x}\right). \quad (8)$$

The existence of this angle leads to the reduction of the effective elastic moduli in the x-direction such that [11, 12]

$$\begin{aligned} E_x^F(\theta) &= 1/[l_\theta^4/E_x^F + (1/G_{xz}^F - 2\nu_{zx}^F/E_x^F)\,l_\theta^2 m_\theta^2 + m_\theta^4/E_z^F] \\ \nu_{yx}^F(\theta) &= \nu_{zx}^F l_\theta^2 + \nu_{yz}^F m_\theta^2 \\ G_{xy}^F(\theta) &= G_{xy}^F l_\theta^2 + G_{yz}^F m_\theta^2 \\ E_y^F(\theta) &= E_y^F = E_z^F, \end{aligned} \quad (9)$$

where $l_\theta = \cos\theta$ and $m_\theta = \sin\theta$. Here, E, G, and ν denote Young's modulus, shear modulus and Poissons' ratio, respectively. The transverse isotropy in the y–z plane of the fill thread has been taken into consideration. Thus, the local stiffness coefficients become

$$Q_{ij}^{F}(\theta) = \begin{bmatrix} E_x^F(\theta)/D_\nu & E_y^F \nu_{yx}^F(\theta)/D_\nu & 0 \\ E_y^F \nu_{yx}^F(\theta)/D_\nu & E_y^F/D_\nu & 0 \\ 0 & 0 & G_{xy}^F(\theta) \end{bmatrix}, \quad (10)$$

where, $i, j = 1, 2, 6$ and $D_\nu = 1 - \nu_{yx}^F(\theta)^2 E_y^F/E_x^F(\theta)$. By substituting Equation 10 into Equations 5 to 7 the local plate stiffness constants can be evaluated.

We define the averaged in-plane compliance of the model under a uniformly applied in-plane stress resultant by

$$\bar{a}_{ij}^{*U} = \frac{2}{n_g a}\int_0^{n_g a/2} a_{ij}^*(x)\,\mathrm{d}x, \quad (11)$$

where the superscript U signifies the fibre undulation model. Since $a_{ij}^*(x)$ is a constant within the straight portion of Fig. 4, Equation 11 can be rewritten as

$$\bar{a}_{ij}^{*U} = \left(1 - \frac{2a_u}{n_g a}\right) a_{ij}^* + \frac{2}{n_g a}\int_{a_0}^{a_2} a_{ij}^*(x)\,\mathrm{d}x, \quad (12)$$

where a_{ij}^* in the first term on the right hand side of Equation 12 denotes the compliance for the straight portion of the threads, namely, a cross-ply laminate and it is independent of x. The other compliance coefficients $\bar{b}_{ij}^{*U}$ and $\bar{d}_{ij}^{*U}$ are obtained in a similar manner.

$$\bar{b}_{ij}^{*U} = \left(1 - \frac{2}{n_g}\right) b_{ij}^* + \frac{2}{n_g a}\int_{a_0}^{a_2} b_{ij}^*(x)\,\mathrm{d}x \quad (13)$$

$$\bar{d}_{ij}^{*U} = \left(1 - \frac{2a_u}{n_g a}\right) d_{ij}^* + \frac{2}{n_g a}\int_{a_0}^{a_2} d_{ij}^*(x)\,\mathrm{d}x. \quad (14)$$

In the case of $n_g = 2$, $\bar{b}_{ij}^{*U}$ vanishes because that $b_{ij}^*(x)$ is an odd function with respect to $x = a/2$, the centre of undulation, due to the form of $h_1(x)$. By inverting the plate stiffness of Equations 5 to 7, explicit expressions of the integrands in Equations 11 to 14 can be obtained. These integrations, however, must be conducted numerically because of their complexity. The final results of the averaged elastic stiffness, $\bar{A}_{ij}^{U}$, $\bar{B}_{ij}^{U}$ and $\bar{D}_{ij}^{U}$, for the entire strip can be reached by inversion of $\bar{a}_{ij}^{*U}$, $\bar{b}_{ij}^{*U}$ and $\bar{d}_{ij}^{*U}$. If this procedure is applied in the warp direction, the balanced properties such as $\bar{A}_{11}^{U} = \bar{A}_{22}^{U}$ can be realized. Numerical results demonstrating the relationship between the in-plane stiffness, $\bar{A}_{11}^{U}$, and $1/n_g$ are given in Fig. 5 for a graphite/epoxy system. Basic material properties are listed in Table I. Here, UB, LB and TA represent the results of the upper and lower bound predictions of the mosaic model [6, 7] and the threadwise analysis, respectively. Circles indicate corresponding finite element results obtained from the compliance values in [11]. Fig. 5 demonstrates that a significant decrease of $\bar{A}_{11}^{U}$ occurs particularly for plain weave ($1/n_g = 0.5$) in comparison with a cross-ply laminate ($1/n_g = 0$). It is also shown that the finite element results are in quite good agreement with simpler analytical results.

3. Analysis of the knee behaviour based on threadwise idealization

The threadwise analysis described above is now extended to the study of the stress–strain behav-

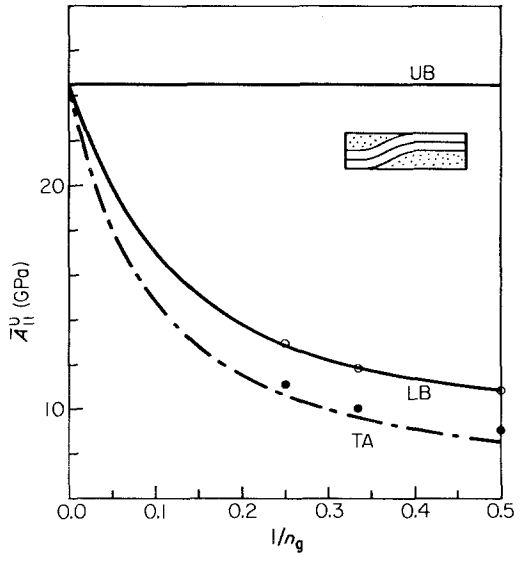

Figure 5 $\bar{A}_{11}^{U}$ against $1/n_g$ for the graphite/epoxy composite, $V_f = 60\%$. Finite element results [11] are indicated by ○ for the mosaic model and by • for the fibre undulation model. —— mosaic model; —·—·— fibre undulation model.

iour of a plain weave composite after initial thread failure, known as a knee phenomenon [4, 8], with some additional assumptions. The essential experimental fact for the knee phenomenon is that the breaking strain in the transverse layer, ϵ_2^b, is much smaller than that of the longitudinal layer in cross-ply laminates [4]. Only the failure of the transverse threads, which occurs in the warp direction in the present model is considered. Thus, a failure criterion based upon maximum strain is adopted and we again confine our attention to the one-dimensional behaviour of fabric composites under an applied N_1 in the following analysis. Then Equation 3a is reduced to

$$\begin{aligned} \epsilon_1^0 &= a_{11}^* N_1 + b_{11}^* M_1 \\ \kappa_1 &= b_{11}^* N_1 + d_{11}^* M_1, \end{aligned} \tag{15}$$

where M_1 is the locally induced moment resultant due to the application of N_1.

By assuming first that no bending deflection by the coupling effect is allowed along the x-axis,

$$\kappa_1 = b_{11}^* N_1 + d_{11}^* M_1 = 0. \tag{16}$$

This assumption can be realized in an exact sense only if the fabric composite plate is symmetrical with respect to its mid-plane. However, in practical multilayer fabric composites, arranged symmetrically to their mid-plane, this assumption is expected to be approximately true. From Equations 15 and 16, we have

$$\epsilon_1^0 = a_{11}^{**} N_1, \tag{17}$$

where $a_{11}^{**} = a_{11}^* - b_{11}^{*2}/d_{11}^*$.

The quantity a_{11}^{**} may be referred to as a modified in-plane compliance and is a function of x. Since N_1 is uniform along the x-direction, $a_{11}^{**}(x)$ represents a strain distribution before the first internal failure. Fig. 6 depicts two examples of the mid-plane strain distribution relative to that at the point $x = 0$ in Fig. 4 and for $a_u = a$. It is easily seen that the fibre undulation causes local softening and that the maximum strain appears at the centre of undulation ($x = a/2$). Also, the strain along the thickness direction at each section is uniform and equal to ϵ_1^0 owing to the classical plate theory and the bending free condition. Although the strain distribution calculated from finite element analysis [11] deviates slightly from the assumed uniform distribution, the present idealization provides a simple method for analysing the knee phenomenon.

We consider that the highest strain in the region exceeds the specified strain ϵ_2^b first, and it immediately leads to the failure of the adjacent area. The damaged area in the warp thread then propagates as the load increases. It is assumed that classical laminate theory is still valid in this

TABLE I Material properties of unidirectional lamina

Material	Graphite/Epoxy [6, 11, 19]		Glass/Polyester [8]	Glass/Polyimide [17, 18]
V_f in threads	65%	60%	60%	50%
E_L	132 GP_a	113 GP_a	47.5 GP_a	41.2 GP_a
E_T	9.31	8.82	15.9	15.7
G_{LT}	4.61	4.46	6.23	5.59
ν_{LT}	0.28	0.3	0.27	0.3
ϵ_2^b	*	*	0.38%	0.5%
Thickness (mm)	0.4	0.4	0.4	0.244

*Strength calculations are not conducted.

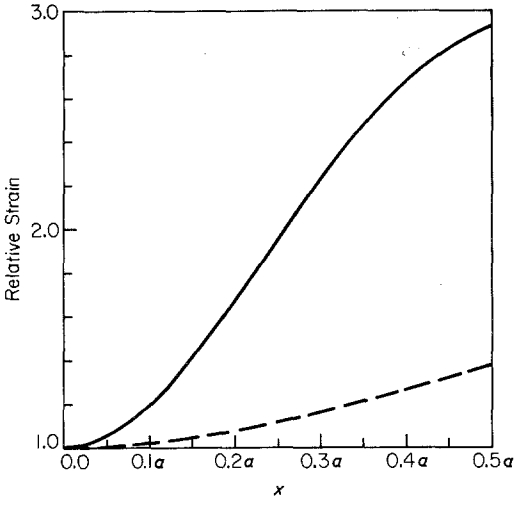

Figure 6 Relative strain distribution along the x-axis in the fibre undulation model under the bending-free condition, $a_u = a$. —— graphite/epoxy; — — glass/polyester.

failure process, and that the effective elastic moduli of such a failed area in the warp threads are much lower than those of a sound area and can be expressed as

$$Q'^{W}_{ij} = \begin{bmatrix} Q^{W}_{11}/100 & Q^{W}_{12}/100 & 0 \\ Q^{W}_{12}/100 & Q^{W}_{22} & 0 \\ 0 & 0 & Q^{W}_{66}/100 \end{bmatrix}. \tag{18}$$

Here, Q'^{W}_{ij} denotes the reduced stiffness of the warp threads after failure, and it is assumed that, with the exception of Q^{W}_{22}, the Q_{ij}s are reduced by a factor of 1/100 to reflect the weakening effect of transverse cracking. The assumption of the applicability of the classical laminate theory implies that we neglect the complex stress and strain fields around the failed region. Such a successive failure process will continue until the lowest strain in the region reaches ϵ_2^b. At that time, all the warp regions are completely failed. Beyond this point, the stress–strain curve becomes a straight line again until the final failure of the fill threads.

Next, consider the case where the restraint on bending is removed. From the classical laminate theory

$$\epsilon(z) = \epsilon_1^0 + z\kappa_1. \tag{19}$$

The strain state under an in-plane stress resultant, N_1, is given by

$$\epsilon(z) = (a^*_{11} + z b^*_{11})N_1. \tag{20}$$

Thus, the strain field under the prescribed N_1 is determined from a^*_{11}, b^*_{11} and z. Since the strain in a section is distributed linearly according to Equation 19, it is necessary to determine the height, h_3, where the strain reaches the critical value, ϵ_2^b. If the strain at the outer edge of the warp threads, $\epsilon_2(h_2)$ according to Equation 19, is larger than ϵ_2^b, we have, for $a_0 \leqq x \leqq a/2$,

$$h_3(x) = h_2 - (h_2 - h_1)\frac{\epsilon_2(h_2) - \epsilon_2^b}{\epsilon_2(h_2) - \epsilon_2(h_1)}. \tag{21}$$

By employing this h_3, the plate stiffness in Equations 5 to 7 needs to be modified after the initial failure. For instance, for $a_0 \leqq x \leqq a/2$,

$$\begin{aligned} A_{ij}(x) = {} & Q^{M}_{ij}[h_1(x) - h_2(x) + h - h_t/2] \\ & + Q^{F}_{ij}(\theta)h_t/2 + Q^{W}_{ij}[h_3(x) - h_1(x)] \\ & + Q'^{W}_{ij}[h_2(x) - h_3(x)]. \end{aligned} \tag{22}$$

Similar modifications to Equation 22 are made for B_{ij} and D_{ij} in Equations 6 and 7.

Fig. 7 presents two numerical examples for a glass/polyester plain weave composite of $a_u = a$ and overall $V_f = 36.8\%$ with and without bending. The finite element analysis by other investigators [8] and their experimental result of acoustic emission [8, 15] are also given. Basic

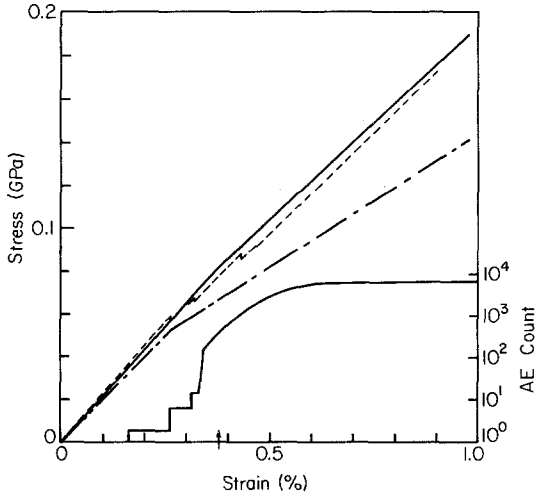

Figure 7 Stress–strain curves for plain weave composites of glass/polyester, $V_f = 36.8\%$ and experimental data of acoustic emission. —— present results for the bending-free condition; —·— present result for the bending unconstrained condition; — — — finite element simulation by Kimpara *et al.* [8]; —— total count in acoustic emission measurement [8, 15]; and an arrow indicates the specified value of ϵ_2^b.

material properties are shown in Table I. The prediction for the bending-free condition compares very favourably with the finite element simulation. It is quite reasonable that the case with bending provides much lower stiffness because it is not subjected to lateral constraints.

In actual plain weave composites, local bending deformation caused by the coupling effect in each interlaced region is constrained by adjacent regions which have opposite signs of B_{ij}. Therefore, as far as plain weave composites are concerned, the threadwise analysis under the bending-free condition should give a reasonable prediction of the behaviour under in-plane loading.

4. Bridging model for satin weaves

The success of the threadwise analysis has led to the concept of a bridging model for general satin composites. Such a model is desirable in view of the fact that the interlaced regions in a satin weave are separated from one another. The hexagonal shape of the repeating unit in a satin weave, as shown in Fig. 8a, is modified to a square shape (Fig. 8b) for simplicity of calculation. A schematic view of the bridging model is shown in Fig. 8c for a repeating unit which consists of the interlaced region and its surrounding areas. This model is

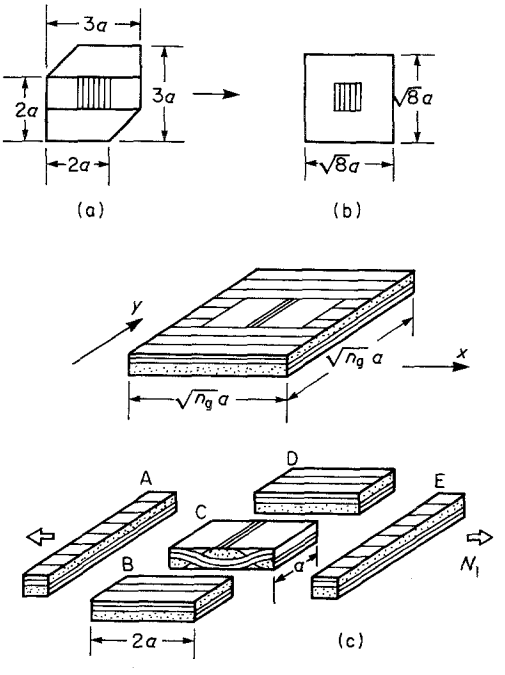

Figure 8 Concept of the bridging model. (a) Shape of the repeating unit of 8 harness satin; (b) modified shape for the repeating unit; (c) idealization for the bridging model.

valid for only satin weaves where $n_g \geqq 4$. The four regions labelled by A, B, D and E consist of straight fill threads, and hence can be regarded as pieces of cross-ply laminates of thickness h_t. Region C has an interlaced structure with an undulated fill thread. Although the undulation and continuity in the warp threads are ignored in this model, the effect is expected to be small because applied load is in the fill direction.

The in-plane stiffness in region C where $n_g = 2$, has been calculated in Section 2 and has been found to be much lower than that of a cross-ply laminate. Therefore, regions B and D carry higher loads than region C and act as bridges for load transfer between regions A and E. It is also assumed here that regions B, C and D have the same averaged mid-plane strain and curvature. Then, the averaged stiffness constants for the regions B, C and D are

$$\bar{A}_{ij} = \frac{1}{\sqrt{n_g}}[(\sqrt{n_g}-1)A_{ij} + \bar{A}_{ij}^{U}]$$

$$\bar{B}_{ij} = \frac{1}{\sqrt{n_g}}(\sqrt{n_g}-1)B_{ij}$$

$$\bar{D}_{ij} = \frac{1}{\sqrt{n_g}}[(\sqrt{n_g}-1)D_{ij} + \bar{D}_{ij}^{U}]. \quad (23)$$

$\bar{A}_{ij}^{U}$ and $\bar{D}_{ij}^{U}$ for the undulated portion C in Fig. 8 are obtained from $\bar{a}_{ij}^{*U}$ and $\bar{d}_{ij}^{*U}$ of Equations 12 and 14, and $\bar{b}_{ij}^{*U} = 0$. A_{ij}, B_{ij} and D_{ij} in Equation 23 for the cross-ply laminates of regions B and D in Fig. 8 are obtained from Equations 3a to d.

It is also postulated that the total in-plane force carried by regions B, C and D is equal to that by region A or E. Then, the following averaged compliance constants are derived

$$\bar{a}_{ij}^{*S} = \frac{1}{\sqrt{n_g}}[2\bar{a}_{ij}^{*} + (\sqrt{n_g}-2)a_{ij}^{*}]$$

$$\bar{b}_{ij}^{*S} = \frac{1}{\sqrt{n_g}}[2\bar{b}_{ij}^{*} + (\sqrt{n_g}-2)b_{ij}^{*}]$$

$$\bar{d}_{ij}^{*S} = \frac{1}{\sqrt{n_g}}[2\bar{d}_{ij}^{*} + (\sqrt{n_g}-2)d_{ij}^{*}] \quad (24)$$

where $\bar{a}_{ij}^{*}$, $\bar{b}_{ij}^{*}$ and $\bar{d}_{ij}^{*}$ are determined by inverting Equation 23 and the quantities with superscript S denote properties of the entire satin plate. Finally, $\bar{A}_{ij}^{S}$, $\bar{B}_{ij}^{S}$ and $\bar{D}_{ij}^{S}$ can be obtained by inverting Equation 24.

The reason why the fibre undulation model is effective for plain weave composites whereas

the bridging model is valid for satin weave composites is explained below. There are no straight thread regions surrounding an interlaced region in the plain weave as can be seen from Fig. 1. Moreover, the threadwise distribution of in-plane stiffness under the bending-free condition is identical in each thread of a plain weave fabric in the loading direction. It can be expected, therefore, that no bridging effect occurs in the plain weave composite, and that each thread carries the same in-plane force. Hence, the threadwise analysis based on the fibre undulation model provides a reasonable prediction of the behaviour of the plain weave composite.

Numerical results for the relationship between the in-plane elastic stiffness $\bar{A}_{11}^{S}$ and $1/n_g$ is indicated in Fig. 9. The properties of constitutive UD laminae are listed in Table I for graphite/epoxy composite [7] with a thread volume fraction of 65%. A prediction by the present theory shows an excellent agreement with experimental results by Zweben and Norman [2]. It should be noted that there is a slight drop of the overall V_f due to the pure resin regions around the undulation. For instance, for a thread V_f of 65%, the average overall V_f in a repeating unit (Fig. 8) for $n_g = 8$, $h_t = h$ and $a_u = a$ is around 62%.

The bridging model and the concept of the successive failure can be combined for analysing the knee behaviour in satin composites. Parallel to the approaches of Section 3, two cases of bending are considered. For the bending free case,

$$\bar{A}_{11}^{*} = 1/\sqrt{n_g}\,\bar{A}_{11}^{*U} + (1 - 1/\sqrt{n_g})A_{11}^{*}, \quad (25)$$

where $A_{11}^{*} = 1/a_{11}^{**}$ and a_{11}^{**} follows the definition in Equation 17. Due to the uniformity of N_1 along the x-direction, we obtain

$$\bar{a}_{11}^{**S} = 2/\sqrt{n_g}\,\bar{a}_{11}^{**} + (1 - 2/\sqrt{n_g})\,a_{11}^{**}$$
$$\bar{A}_{11}^{*S} = 1/\bar{a}_{11}^{**S}, \quad (26)$$

where $\bar{a}_{11}^{**} = 1/\bar{A}_{11}^{*}$. Similar expressions for the unconstrained bending case can also be obtained but are omitted here. The rest of the procedure for examining the knee phenomenon is quite similar to that of Section 3. The initial failure of the warp threads occurs at the point of highest strain, for example, the centre of the undulation in the bending free case. Also, since there are regions of uniform strains such as the bridging zones in this model, the entire area of those regions may fail simultaneously, according to the present assumptions.

Fig. 10 compares numerical and experimental results for stress–strain curves of 8 harness satin fabric plates of glass/polyimide composites. Basic material properties are also indicated in Table I, where certain values are estimated from matrix

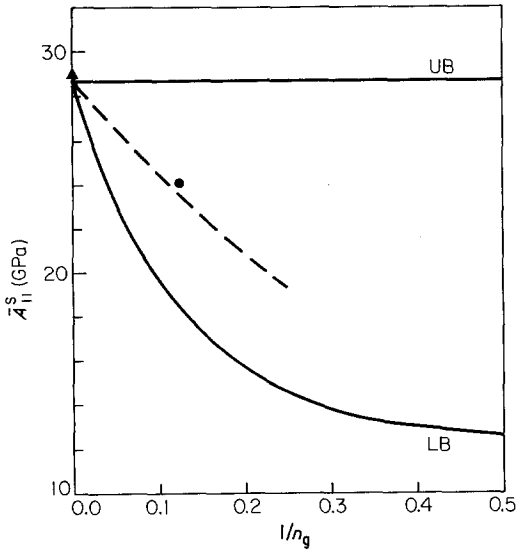

Figure 9 $\bar{A}_{11}^{S}$ against $1/n_g$ for a graphite/epoxy system, $V_f = 65\%$. —— upper and lower bounds; — — bridging model solution; ▲ and ●, experimental results for a cross-ply laminate and 8 harness satin, respectively [2].

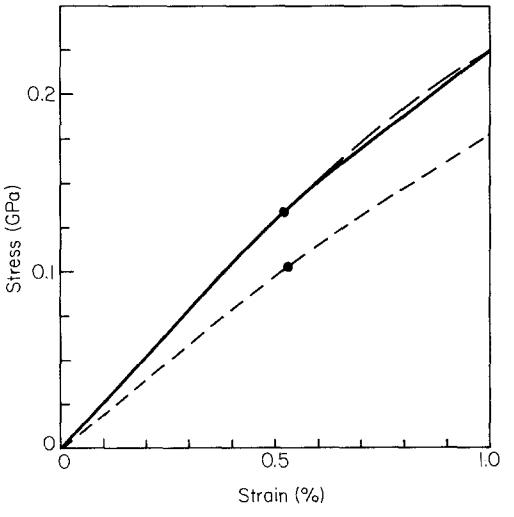

Figure 10 Theoretical and experimental stress–strain curves for a glass/polyimide composite, $V_f = 50\%$ in threads. —— bridging model solution without bending for 8 harness satin (overall $V_f = 47.7\%$); – – – fibre undulation model solution without bending for plain weave (overall $V_f = 40.9\%$); — — an experimental curve from [17]; • knee points.

data [6, 18]. The experimental curve is reproduced from [17]. Since test pieces were curved nearly symmetrically with respect to their mid-planes, the bending free analysis is selected for comparison. It can be seen that the agreement is quite good, particularly for strain values up to the point of the knee. A theoretical curve for the plain weave composite of the same material is also shown in Fig. 10. We define a knee point by a deviation of 0.01% in strain from the linear strain. Then, we observe that knee stress in the 8 harness satin is higher than that of the plain weave although knee strains are nearly identical. It can be concluded that the elastic stiffness and knee stress in satin composites are higher than those in plain wave composites due to the presence of the bridging regions.

5. Conclusions

(1) A threadwise analysis of fabric composites in which fibre continuity and undulations are considered has been conducted. The fibre undulation model based upon a threadwise strip provides better predictability than the mosaic model.

(2) The results of the threadwise analysis for in-plane elastic stiffness of fabric composites exhibit considerable softening as compared to cross-ply laminates. This approach is particularly suited for predicting elastic properties of plain weave composites and the theory compares very favourably with finite element analysis.

(3) The threadwise analysis has been applied to examine the knee phenomenon of plain weave composites. The predicted knee behaviour of a glass/polyester composite under the bending free assumption shows an excellent agreement with the stress–strain curve obtained by other workers using the finite element analysis.

(4) A bridging model also has been developed to examine the stiffness and strength of general satin composites. The interlaced regions in a satin fabric are separated from one another by the non-interlaced regions. Since the regions with straight threads surrounding an interlaced region have higher in-plane stiffness than the latter, they carry higher loads and play the role of load transferring bridges.

(5) The initial elastic stiffness of satin composites can be predicted by the bridging model. The present analysis of an 8 harness satin composite of graphite/epoxy demonstrates good agreement with experimental data obtained by other workers, for the fabric and for a cross-ply laminate as the limiting case.

(6) The concept of successive failure of the warp threads and the bridging idealization have been combined to study the knee behaviour in satin composites. The theoretical results for an 8 harness satin reinforced glass/polyimide composite compares extremely well with the experimental curve. It has been concluded that the bridging regions surrounding the interlaced regions are responsible for the higher stiffness and knee stress in satin composites than those in plain weave composites.

Acknowledgements

This work is sponsored by the US Army Research Office. The authors also wish to thank Mr Y. Zto of Kawasaki Heavy Industries LTD for sharing with us his experimental results on glass/polyimide composites.

References

1. C. ZWEBEN, Advanced Composites: A Revolution for the Designer, AIAA 50th Annual Meeting. "Learn from the Masters" Series, May 1981.
2. C. ZWEBEN and J. C. NORMAN, *SAMPE Q.* July (1976) 1.
3. A. NISHIMURA, Proceedings of 10th Symposium on Materials in Aerospace Technology, Tokyo, Japan, Feb. 1980 (in Japanese).
4. S. W. TSAI, NASA CR-224, April, 1965.
5. E. MILLER, "Textiles; Properties and Behaviour" revised edn. (B. T. Batsford, London, 1976).
6. T. ISHIKAWA, *Fibre Sci. Technol.* **15** (1981) 127.
7. T. ISHIKAWA and T. W. CHOU, *J. Composite Mater.* **16** (1982) 2.
8. I. KIMPARA, A. HAMAMOTO and M. TAKEHANA, Trans. JSCM **3** (1977) 21.
9. T. HIRAI and T. SENBA, "On the Mechanical Behaviour of Fabric-Strengthened Composites Considering Three-Dimensional Cross-Linked Structure," ICCM 3, Paris (1980), p. 357.
10. J. KAVELKA, "Thermal Expansion of Composites with Canvas-Type Reinforcement and Polymer Matrix," ICCM 3, Paris (1980), p. 770.
11. T. ISHIKAWA and T. W. CHOU, *AIAAJ* in press.
12. R. M. JONES, "Mechanics of Composite Materials" (Scripta, Washington, D.C., 1975).
13. J. M. WHITNEY and A. W. LEISSA, *J. Appl. Mech.* **36** (1969) 261.
14. T. HAYASHI (ed.), "Fukugo-Zairyo Kogaku", (Composite Material Technology) (Nikka-giren, Tokyo, 1971) (in Japanese).
15. J. KIMPARA and M. TAKEHANA, Proceedings of the 2nd Acoustic Emission Symposium, Tokyo, 1974, Session 9/2-20.
16. J. C. HALPIN, *J. Composite Mater.* **6** (1972) 208.

17. Kawasaki Heavy Industry LTD, private communication.
18. Rhône-Poulenc Corp., "Catalogue of Polyimide Resin".
19. T. ISHIKAWA, K. KOYAMA and S. KOBAYASHI, *J. Composite Mater.* **11** (1977) 332.

Received 2 March
and accepted 22 March 1982